Advanced Composite Materials
Publication details, including instructions for authors and subscription information:
http://www.tandfonline.com/loi/tacm20

Incorporating Aspect Ratio in a New Modeling Approach for Strengthening of MMCs and its Extension from Micro to Nano Scale

A. Zehtab Yazdi [a] , R. Bagheri [b] , S. M. Zebarjad [c] & Z Razavi Hesabi [d]

[a] Materials Science and Engineering Department, Sharif University of Technology, P.O. Box 11365-9466, Tehran, Iran

[b] Materials Science and Engineering Department, Sharif University of Technology, P.O. Box 11365-9466, Tehran, Iran

[c] Materials Science and Engineering Department, Engineering Faculty, Ferdowsi University of Mashhad, P.O. Box 91775-111, Mashhad, Iran

[d] Materials Science and Engineering Department, Sharif University of Technology, P.O. Box 11365-9466, Tehran, Iran

Version of record first published: 02 Apr 2012.

To cite this article: A. Zehtab Yazdi , R. Bagheri , S. M. Zebarjad & Z Razavi Hesabi (2010): Incorporating Aspect Ratio in a New Modeling Approach for Strengthening of MMCs and its Extension from Micro to Nano Scale, Advanced Composite Materials, 19:4, 299-316

To link to this article: http://dx.doi.org/10.1163/092430409X12605406698390

VSP

Advanced Composite Materials 19 (2010) 299–316

ADVANCED COMPOSITE MATERIALS
brill.nl/acm

Incorporating Aspect Ratio in a New Modeling Approach for Strengthening of MMCs and its Extension from Micro to Nano Scale

A. Zehtab Yazdi [a], **R. Bagheri** [a,*], **S. M. Zebarjad** [b] **and Z. Razavi Hesabi** [a]

[a] Materials Science and Engineering Department, Sharif University of Technology, P. O. Box 11365-9466, Tehran, Iran

[b] Materials Science and Engineering Department, Engineering Faculty, Ferdowsi University of Mashhad, P. O. Box 91775-111, Mashhad, Iran

Received 11 March 2009; accepted 28 August 2009

Abstract

The strengthening behavior of particle reinforced metal–matrix composites is primarily attributed to the dislocation strengthening effect and the load transfer effect. To account for these two effects in a unified way, a new multi-scale approach is developed in this paper incorporating the aspect ratio effect into the geometrically necessary dislocation strengthening relationships. By making use of this multi-scale approach, the deformation behavior of metal–matrix composites (MMCs) and metal–matrix nanocomposites (MMNCs) as a function of size, volume fraction, aspect ratio, etc. of the particles has been investigated. Comparison with the previously proposed models and the available experimental results reported in the literature for both MMCs and MMNCs systems demonstrates the superiority of the proposed model.

Keywords

Metal–matrix composites (MMCs), strength, multi-scale modeling

1. Introduction

Metal–matrix composites (MMCs) have the potential to provide desirable mechanical properties including high specific stiffness, strength and high creep resistance [1]. These properties make MMCs strong candidates for using in aerospace, defense and automobile applications. Metal–matrix nanocomposites (MMNCs) are most promising in producing balanced mechanical properties between nano and micro structured materials, i.e., enhanced hardness and Young's modulus, 0.2% yield strength, ultimate tensile strength and ductility [2–7], due to the addition of

* To whom correspondence should be addressed. E-mail: rezabagh@sharif.edu
Edited by the JSCM

 DOI:10.1163/092430409X12605406698390

nano-sized reinforcement particles into the matrix. It is generally recognized that direct and indirect strengthening may occur in both MMCs and MMNCs [8]. Direct strengthening is due to load transfer from the metal–matrix to the reinforcing particle whereas indirect strengthening results from the influence of reinforcement on matrix microstructure or deformation mode. For example, indirect strengthening can appear because of dislocation generation due to mismatching of both elastic modulus (EM) and coefficient of thermal expansion (CTE) of the reinforcement and the matrix [8]. During the past two decades, several attempts have been made to explore the relationship between microstructure and the deformation behavior in MMCs [9–22]. Continuum models including the cell model [9, 10], the modified shear lag theory [11] and homogenization models [12] provide a dependence of flow stress on volume fraction of reinforcing particles, but not on their size. It seems the drawback of the continuum approach is that it ignores the influence of location of particles, grain size and dislocation density on the micromechanics of deformation and strengthening mechanisms [13]. On the other hand, dislocation based models [14, 15] neglect the load-bearing term of strengthening.

In the meantime, Ramakrishnan [16] proposed an analytical model for predicting the yield strength of the micro-sized particulate-reinforced MMCs. He used a composite sphere model for the intra-granular type of MMCs and incorporating two improvement parameters associated with the dislocation strengthening of the matrix and the load-bearing effect of the reinforcement. The model presented an incorporation of both continuum and micromechanics approaches to predict the low-cycle fatigue life of discontinuous reinforced MMCs [17, 18]. Dai *et al.* [19, 20] proposed a hybrid approach by incorporating the geometrically necessary dislocation effect into the micromechanical scheme and investigated the strengthening behavior of MMCs. However, the model neglected the effects of aspect ratio of the reinforcement and was applicable only for MMCs containing micron-size particles. In the class of MMNCs, Zhang and Chen [21, 22] developed an analytical model for predicting the yield strength of MMNCs. Three strengthening effects involving (i) Orowan strengthening mechanism, (ii) enhanced dislocation density due to the residual plastic strain caused by the difference in the coefficients of thermal expansion between the matrix and the particles and (iii) load-bearing effect have been taken into account in the model. Despite good agreement between the experiment and the modeling results, the applicability on the micron-size particles was not investigated. Indeed, the effects of aspect ratio of the reinforcement and enhanced dislocation density due to the elastic modulus (EM) mismatch were not considered.

According to the literature survey done by the authors, presenting a model to predict the yield strength of both MMCs and MMNCs can fill the literature gap in this field. Therefore, in the current research, we present the first multi-scale approach in modeling of the strengthening behavior. Considering the effects of size, volume fraction, aspect ratio and properties of the reinforcement concurrently in the proposed analytical model will be the unique and advantageous aspect of this

approach. Also, the result of the current model will be compared with those of previous analytical models as well as the published experimental results.

2. The Model Development

2.1. Background

It is clear that the microstructure and properties of the composite matrix or *in situ* matrix may be significantly different from those of the unreinforced matrix alloy. With addition of the reinforcing phase, the geometrically necessary dislocations are generated to accommodate the mismatch of plastic deformation in the matrix. The presence of particles induces an inhomogeneous deformation pattern in MMCs and high dislocation density in the composite matrix [23]. Calculations of the dislocation density due to EM mismatch as a function of size, volume fraction and in particular, aspect ratio is the most important step in this paper. At the foremost in this paper, the total number of dislocation loops per unit volume (N^{T}) for a cylindrical particle is estimated. Consider a cube shaped cell of matrix containing a single cylindrical particle subjected to the plastic shear strain γ (Fig. 1). The particle was removed from the cell and the cell was deformed uniformly. Afterwards, the particle was replaced into the formed hole. It is worth noting that the amount of particle deformation was neglected in comparison to the plastic strain in the matrix. Thus, the compatibility condition requires that the hole be deformed back to its original shape. Many possible sets of displacements can accomplish this. The simplest way is shearing the part of the matrix surrounding the hole to back by an amount of γ as shown in Fig. 2(a). These displacements are achieved by inserting *n shear loops*, surrounding the particles as shown. The dislocation array is acceptable only if the local yield stress is not exceeded anywhere. In this school of thought, the nucleation of new dislocations from the particle matrix interface or the cross slip of dislocations of the array are neglected. Ashby *et al*. [23] showed that new dislocations

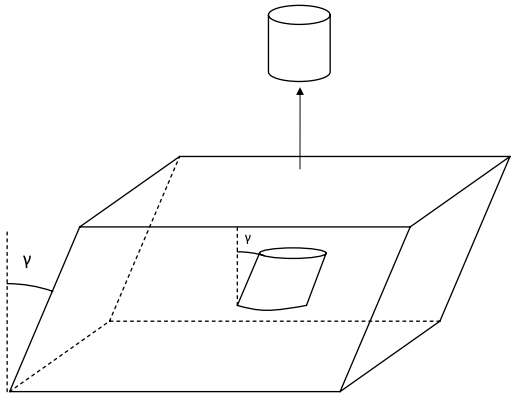

Figure 1. A cube cell containing a cylindrical particle that is subjected to the plastic shear strain γ.

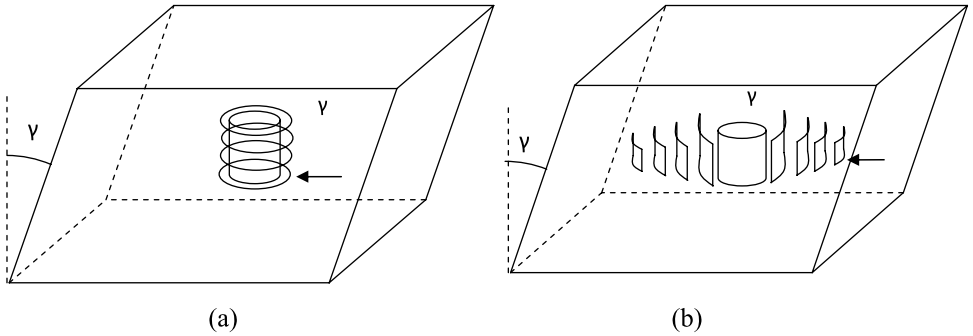

Figure 2. The compatibility methods that allow the hole to be deformed back to its original shape by inserting an array of (a) shear loops and (b) prismatic loops.

can often be generated from the interface between the particle and matrix. Alternatively, the necessary displacements can be obtained by inserting prismatic loops as shown in Fig. 2(b). Despite the previous model, the local yield stress in this model can be exceeded and used as a base of calculations in the current analytical model. Ashby and Johnson [24] applied this approach to the cubic particles and simply predicted the dislocation density as a function of shear strain, volume fraction and size of the particles. In contrast, in the current research the particle shape is selected as a cylinder and the variations of aspect ratio of the particle are considered on the model (Section 2.2): this is one of the important contributions of this investigation. Although the complexity of the presented model is much greater than that of Ashby and Johnson [24], it will be shown that the current model is more flexible and compatible compared with the conventional models and the experimental results, respectively.

2.2. Improvement

The prismatic loops shown in Fig. 2(b) restore the hole to its original shape by removing material from the right and adding to the left. Generally, the relationship between N^{T}, N_{V} (the total number of particles) and n^{T} (the total number of loops per particle) can be expressed as [19]:

$$N^{\mathrm{T}} = N_{\mathrm{V}} \times n^{\mathrm{T}}. \tag{1}$$

Also, N_{V} and n^{T} are given by [23]:

$$n^{\mathrm{T}} = \frac{V_{\mathrm{m}}}{\bar{A}b}, \tag{2}$$

$$N_{\mathrm{V}} = \frac{f}{V_{\mathrm{p}}}, \tag{3}$$

where V_{m}, $\bar{A}$, b, f and V_{p} are the mismatch volume, the average area of the loops, Burgers vector of dislocations in the matrix, the volume fraction of the reinforce-

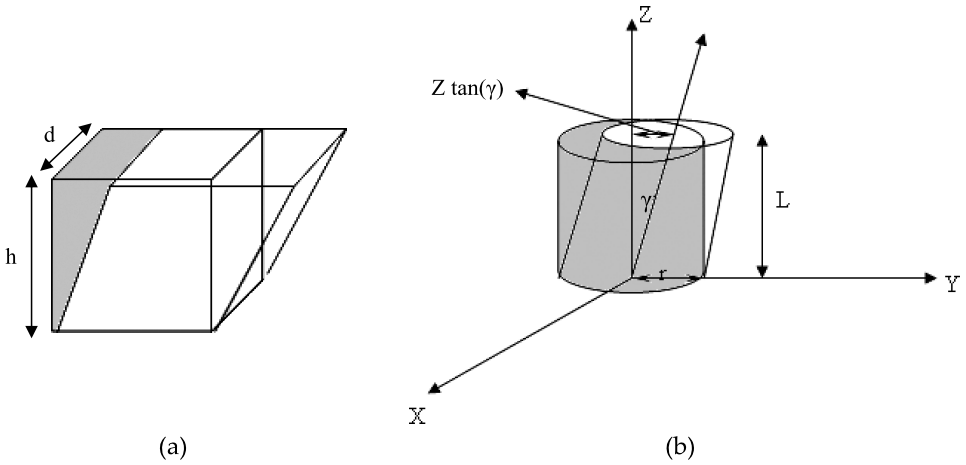

Figure 3. The representative mismatch volume and geometrical parameters for (a) cubic shaped particle and (b) cylindrical shaped particle.

ment and the volume of the particle, respectively. Therefore, N^{T} can be written as:

$$N^{\mathrm{T}} = \frac{f}{b} \times \frac{V_{\mathrm{m}}}{V_{\mathrm{p}}\bar{A}}. \tag{4}$$

As equation (4) shows, the first term (f/b) depends on the properties and processing conditions of the matrix and reinforcement, respectively. But the second term $(V_{\mathrm{m}}/V_{\mathrm{p}}\bar{A})$ depends on the shape of the particle. In this paper, the second part of equation (4) is taken into account. As stated above, Ashby and Johnson [24] consider the simple cubic shaped particle as shown in Fig. 3(a). Therefore, the mismatch volume which is shaded on the left side of the particle in Fig. 3(a), has been considered according to [24]:

$$V_{\mathrm{m}}^{\mathrm{cb.}} = h^2 d \tan\gamma = (AR) d^3 \tan\gamma, \tag{5}$$

where d and h are shown in Fig. 3(a). Aspect ratio (AR) of the cubic particle is also defined as h/d ratio. In the case of $AR = 1$, the mismatch volume can be simply rewritten as

$$V_{\mathrm{m}}^{\mathrm{cb.}} = d^3 \tan\gamma, \tag{6}$$

In contrast to the previous model [24], the mismatch volume (V_{m}) of the cylindrical shaped particle as shown in Fig. 3(b) can be calculated using complex triple integration (volumetric integration). As a result of the calculations for the cylindrical particle, $V_{\mathrm{m}}^{\mathrm{cl.}}$ is:

$$V_{\mathrm{m}}^{\mathrm{cl.}} = \int_0^L 2r^2 \left(\frac{z\tan(\gamma)}{2r^2} \sqrt{4r^2 - z^2\tan^2(\gamma)} + 2\sin^{-1}\left(\frac{z\tan(\gamma)}{2r} \right) \right) \mathrm{d}z. \tag{7}$$

And, thus, $V_{\mathrm{m}}^{\mathrm{cl.}}$ can be written as:

$$V_{\mathrm{m}}^{\mathrm{cl.}} = -\frac{r^3}{6\tan\gamma}\left[(4-c^2\tan^2\gamma)^{3/2} - 12c\tan\gamma\sin^{-1}\left(\frac{c\tan\gamma}{2}\right) - 12(4-c^2\tan^2\gamma)^{1/2} + 16\right], \tag{8}$$

where r is the radius of the cylindrical particle and c is related to the aspect ratio (AR) by $AR = 2c$. It is assumed that the relationship between L (length) and r (radius) of the cylindrical particle is $L = cr$ and particle area is constant and remains as a circle.

The other parts of the second term ($V_{\mathrm{p}}\bar{A}$) in the equation (4) were calculated for both particle shapes. As Dai *et al*. [19] and Ashby and Johnson [24] mentioned, all loops may not have the same size, but the geometry condition requires that their average area ($\bar{A}$) be close to $0.5d^2$ for cube shaped particle. In the present model, $\bar{A}$ can be considered equal to πrL or πcr^2 (assuming $L = cr$) in the same way. At constant volume fraction of the reinforcement, the relationship between d and r for cubic and cylindrical particles, respectively, can be expressed as follows:

$$d^3 = \pi cr^3 \rightarrow d = r\sqrt[3]{\pi c}. \tag{9}$$

Combining equation (4) and equation (8) and nominate the term of $\frac{V_{\mathrm{m}}d^3}{V_{\mathrm{p}}\bar{A}}$ as φ factor, N^{T} can be written as:

$$N^{\mathrm{T}} = \frac{f}{b}\times\frac{\varphi}{d^2}. \tag{10}$$

This factor can be calculated for both particle shapes as follows:

$$\varphi^{\mathrm{cb.}} = 2\tan\gamma \tag{11}$$

$$\varphi^{\mathrm{cl.}} = \frac{-\left[(4-c^2\tan^2\gamma)^{3/2} - 12c\tan\gamma\sin^{-1}\left(\frac{c\tan\gamma}{2}\right) - 12(4-c^2\tan^2\gamma)^{1/2} + 16\right]}{6(\pi c)^{4/3}\tan\gamma}. \tag{12}$$

Considering aspect ratio of the cylindrical reinforcement as a variable parameter in equation (12), unlike the cubic shape, is one of the most distinctive characteristics of the proposed model which has not been reported before. This parameter makes the model more flexible and compatible with the experimental results (as will be shown in Section 3) than the previous models [19, 24].

2.3. Dislocation Density Determination

The increase in the dislocation density in the composite matrix is assumed to be mainly due to the elastic modulus (EM) and the coefficient of thermal expansion (CTE) mismatches between the matrix and the reinforcement. The generated dislocations by EM and CTE mismatches can be considered as two types of the

geometrically necessary dislocation [25]. It should be noted that because the current model considers various particle shapes from disk-like to needle-like, the following calculations have been done only for the cylindrical particle, and the cubic particle has been disregarded.

If the length of each dislocation loop is taken as πd, then the geometrically necessary dislocation density due to EM mismatching (ρ^{EM}) in the case of cylindrical shape particle is given by [19]:

$$\rho_{\mathrm{G}}^{\mathrm{EM}} = N^{\mathrm{T}} \times \pi d. \tag{13}$$

Introducing equation (10) into equation (13) and assuming $d \approx d_{\mathrm{p}}$ leads to:

$$\rho_{\mathrm{G}}^{\mathrm{EM}} = \frac{1}{b} \times \frac{\varphi^{\mathrm{cl.}} f \pi}{d_{\mathrm{p}}}. \tag{14}$$

As equation (14) shows, $\rho_{\mathrm{G}}^{\mathrm{EM}}$ is a function of both volume fraction (f) and size of the reinforcement (d_{p}), as well as shear strain (γ) and aspect ratio of the cylindrical particle ($2c$) which is included in the φ factor. Typical great difference between the coefficient of thermal expansions (CTEs) of the matrix and the ceramic reinforcement, $\Delta\alpha$, plays an important role in the deformation behavior of metal–matrix composites. The CTE of a ceramic reinforcement is smaller than that of most metallic matrices. When the metal–matrix composite is cooled down from a higher processing temperature to the room temperature, misfit strains appear because of differential thermal contraction at the interface. These strains induce thermal stresses that may be higher than the yield stress of the matrix. The thermal stresses may be sufficient to generate new dislocations at the interfaces between the matrix and the reinforcements [26]. Therefore, after the composite is cooled, the dislocation density in the matrix will increase. The density of the newly formed dislocations, in the vicinity of reinforcement (fibers or particles), can be calculated as follows [15]:

$$\rho_{\mathrm{G}}^{\mathrm{CTE}} = \frac{4\Delta\alpha\Delta T f}{b(1-f)}\left(\frac{1}{t_1} + \frac{1}{t_2} + \frac{1}{t_3}\right), \tag{15}$$

where ΔT is the difference between the processing and test temperatures. In equation (15), t_1, t_2 and t_3 represent the three dimensions of the particles. In the case of cylindrical particles, $t_1 = t_2 = 2r$ and $t_3 = L$. By substituting the parameters into equation (15) and considering $L = cr$, $\rho_{\mathrm{G}}^{\mathrm{CTE}}$ becomes:

$$\rho_{\mathrm{G}}^{\mathrm{CTE}} = \frac{8\Delta\alpha\Delta T}{b} \times \frac{f(c+1)}{cd_{\mathrm{p}}(1-f)}. \tag{16}$$

2.4. Strengthening Behavior

An increase in dislocation density in MMCs can lead to the *in situ* matrix being of higher yield strength over the unreinforced metal–matrix. For this case, the yield strength of the *in situ* matrix is given by [27]:

$$\sigma_{\mathrm{my}} = \sigma_{\mathrm{m}} + \Delta\sigma, \tag{17}$$

where σ_{my} and σ_m are the yield strength of the *in situ* matrix and the unreinforced matrices, respectively. While the total increment in yield stress of the *in situ* matrix ($\Delta\sigma$) can be estimated by [27]:

$$\Delta\sigma = \sqrt{(\Delta\sigma_{EM})^2 + (\Delta\sigma_{CTE})^2 + (\Delta\sigma_{LT})^2}. \tag{18}$$

The increments in yield stress of the *in situ* matrix due to EM ($\Delta\sigma_{EM}$) and CTE ($\Delta\sigma_{CTE}$) stresses are determined by Taylor dislocation strengthening relations [27]:

$$\Delta\sigma_{EM} = \sqrt{3}\alpha\mu_m b\sqrt{\rho_G^{EM}}, \tag{19}$$

$$\Delta\sigma_{CTE} = \sqrt{3}\beta\mu_m b\sqrt{\rho_G^{CTE}}, \tag{20}$$

where μ_m is the shear modulus of the matrix and α and β (two dislocation strengthening coefficients) are taken, respectively, to be 0.5 and 1.25 in subsequent calculations [27]. In addition, one of the most important continuum mechanisms, e.g., *load-bearing effect*, should be considered in this analytical model. The load transfer from matrix to reinforcing phase is maintained by the interface. The shear lag theory assumes that the load transfer occurs between reinforcement with high aspect ratio and the matrix *via* the shear stress at the reinforcement–matrix interface. According to this mechanism, fiber acts as reinforcement and carries part of the load. An increase in the yield stress due to load transfer mechanism ($\Delta\sigma_{LT}$) may be given by [28]:

$$\Delta\sigma_{LT} = \sigma_m f\frac{(c+2)}{8}. \tag{21}$$

Substituting equations (18)–(21) into equation (17) reveals that the total increment in yield stress of *in situ* matrix ($\Delta\sigma$) is a function of three different types of parameters. The first group of these parameters conveys the properties of the matrix and the reinforcement, e.g., b, μ_m, $\Delta\alpha$ and ΔT. The second is conveying the geometry of the reinforcement such as c and d_p. The last one discloses the processing conditions, e.g., f and γ. Consequently, the effects of the geometry and processing parameters in the given MMCs system have been investigated. Figure 4 presents the analytical results of the effect of the volume fraction (f), size (d_p) and aspect ratio ($2c$) of the particles on the total incremental in yield strength ($\Delta\sigma$) of Al–SiC system based on equation (18). The pertinent mechanical and physical properties for both kinds of materials (Al as matrix and SiC as reinforcement) are listed in Table 1 [29]. It is noted that the value of the applied shear strain (γ) quoted in equation (11) is about 30% [25]. As shown in Fig. 4, with decreasing size of the particles, the strengthening effect in MMCs increase. This effect is significant in the particle sizes smaller than of about 5 μm. In addition, the favored strengthening behavior can be observed with increasing aspect ratio ($2c$), even in the larger size of the reinforcement. The strengthening effect in the aspect ratio ($2c$) < 1 has been studied and the trend same as $2c > 1$ was observed. In the case that $2c < 1$, the

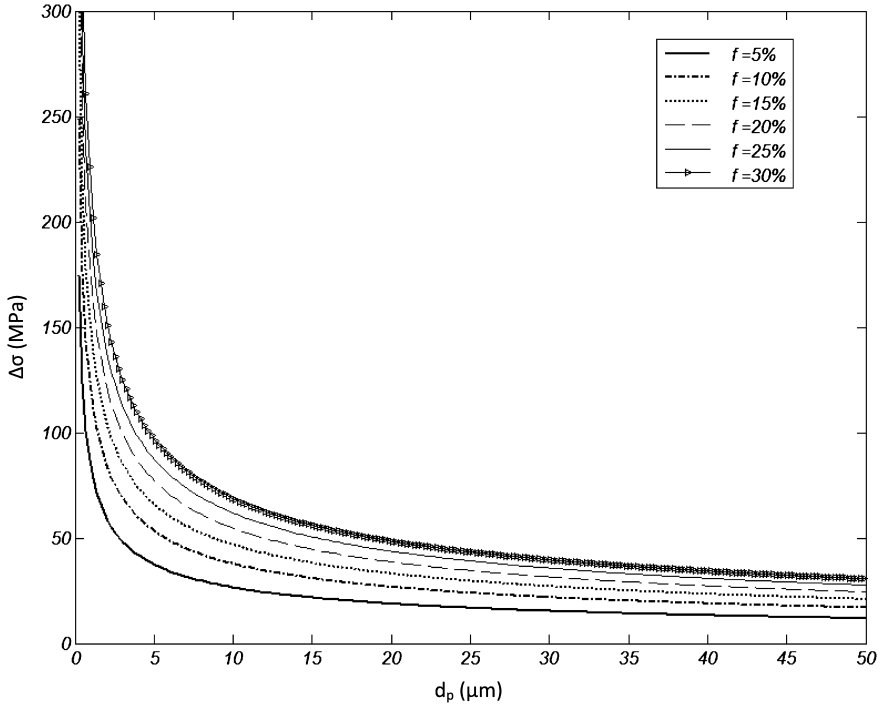

(a)

Figure 4. The total incremental increase in yield strength ($\Delta\sigma$) as a function of particle size (d_p) and particle volume fraction (f) of the reinforcement in Al–SiC micro-composite for different aspect ratios include: (a) $AR = 1$, (b) $AR = 10$, (c) $AR = 25$ and (d) $AR = 50$.

shape of the particle may be disk-like or platelet. Also, it can be seen from Fig. 4, that the volume fraction of the reinforcement in the smaller particle size (d_p) and larger aspect ratio ($2c$) has the stronger outcomes on $\Delta\sigma$ compared to that of the larger particle size and smaller aspect ratio.

3. Comparison of the Model and Discussion

To check the utility of the current hybrid model, comparisons between the presented model, the conventional models [19, 21, 22] and the experimental results [14, 19] are made in this section. The new model shows both flexibility and compatibility compared to the conventional models and experimental data, respectively.

3.1. A356–T6/SiC Microcomposite

Here, the incremental increase in true yield stress of A356–T6 aluminum alloy due to decrease of particle size (SiC) from 16 μm to 8 μm ($\Delta\sigma_{16-8\ \mu m}$) has been calculated using the new approach, as shown in Fig. 5. Moreover, comparisons between the increment micromechanical scheme and experimental results [19] have been made in the figure. In this case, the volume fraction (f) and aspect ratio ($2c$) of

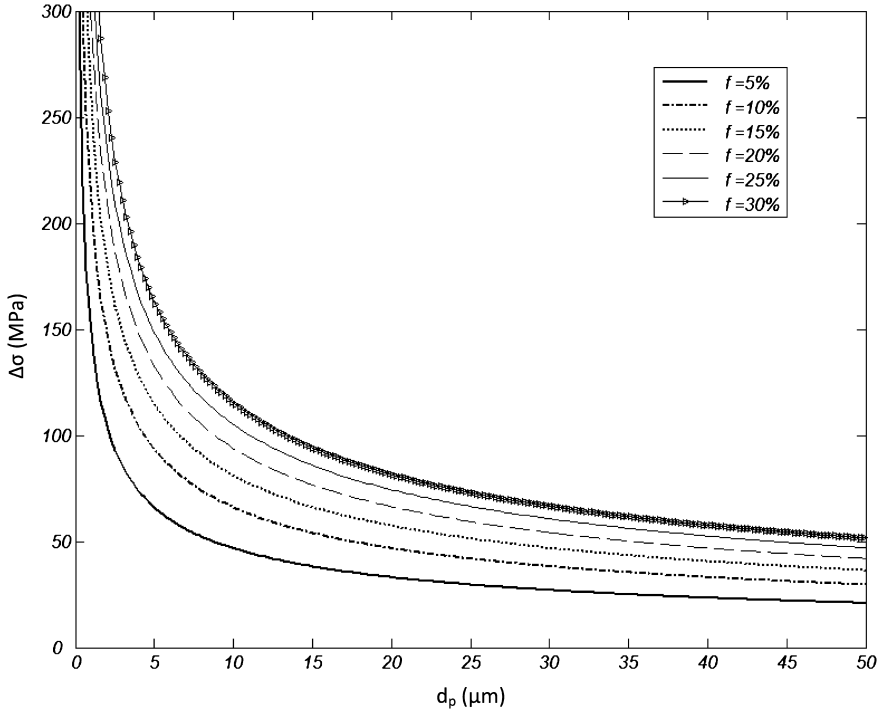

(b)

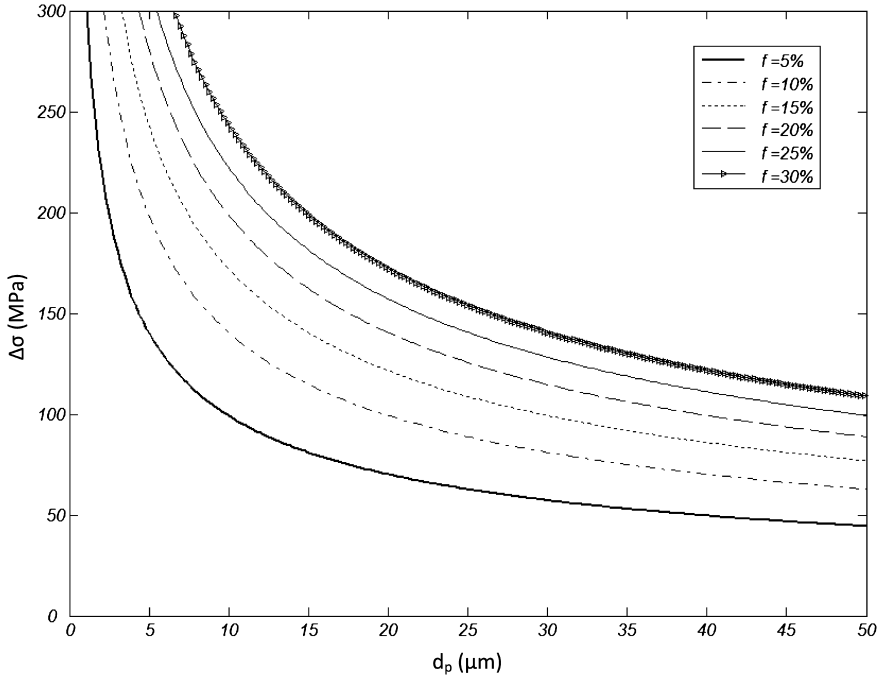

(c)

Figure 4. (Continued.)

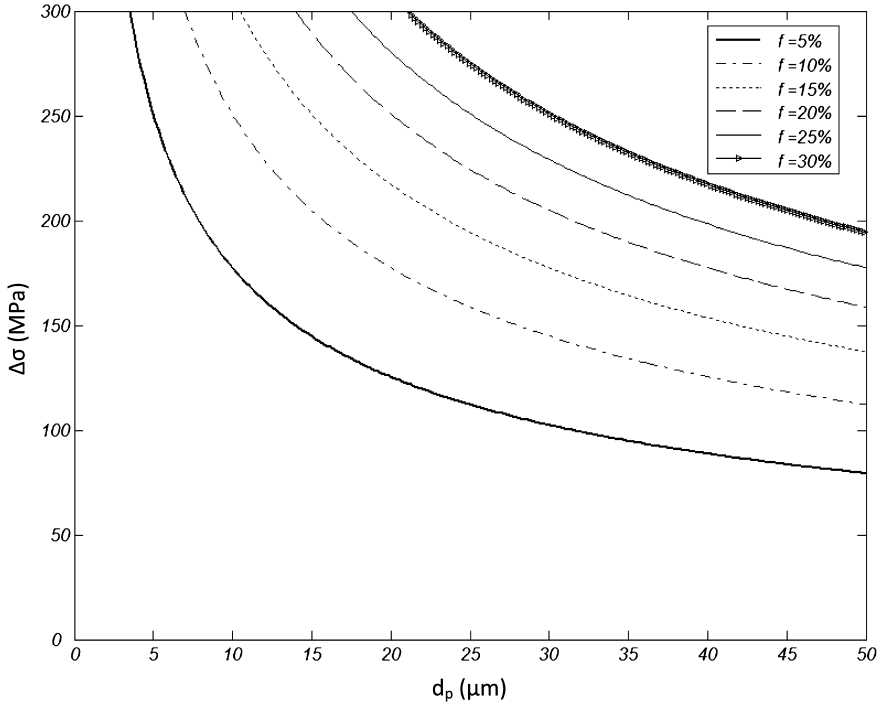

(d)

Figure 4. (Continued.)

Table 1.
The mechanical and thermal properties of Al–SiC composite [29]

Property	b (°A)	α_p (1/°C)	α_m (1/°C)	$T_{processing}$ (°C)	T_{test} (°C)	μ_m (GPa)	σ_m (MPa)
Values	2.83	5×10^{-6}	24×10^{-6}	220	20	27	40

the reinforcement within the new proposed model have been considered 0.15 and 1, respectively. It has been noted that the relationship between the local shear strain (γ) and the overall tensile strain (ε) must be determined according to the following linear equation:

$$\gamma = k\varepsilon, \tag{22}$$

where k is a fitting parameter and should be calculated based on only one set of experimental data. This parameter has a strong dependency to the scrutinized system of MMCs and takes a single value for the examined MMCs. Values of k factor for A356T6–SiC composite and the subsequent MMC or MMNC systems have been presented in Table 2.

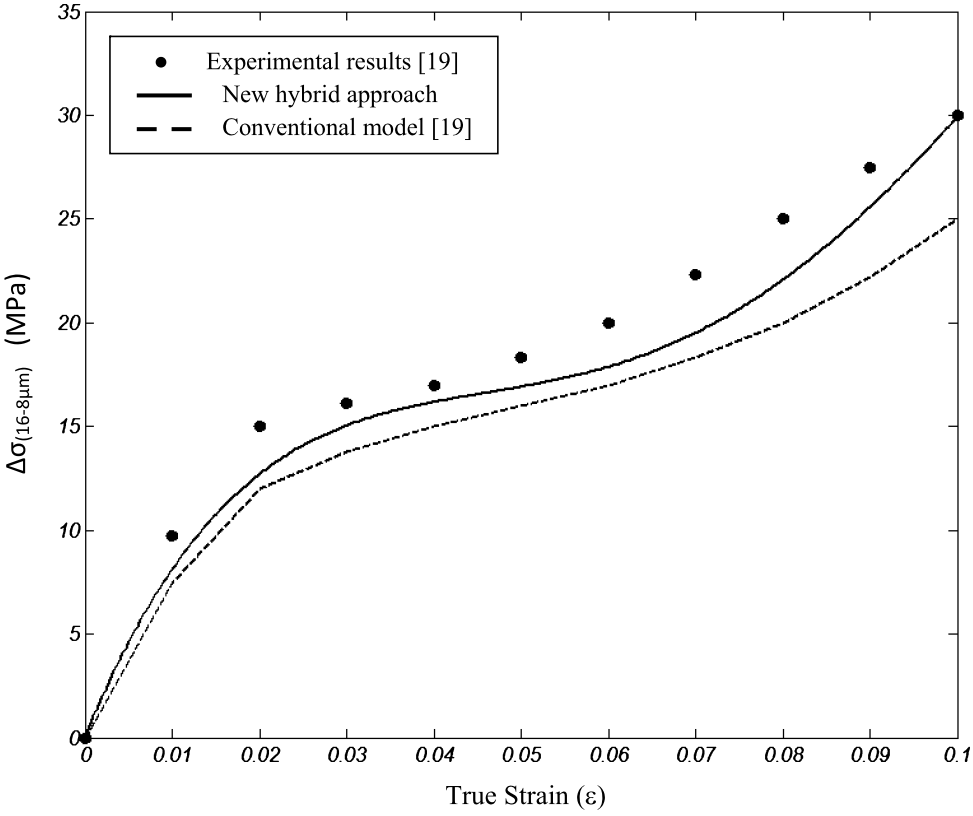

Figure 5. The total incremental increase in yield strength ($\Delta\sigma$) due to decrease of particle size (16–8 μm) *versus* true strain in A356T6–SiC micro-composite. Comparisons with the conventional model and experimental results [19] have been made.

Table 2.
Values of the correction factor (k) are calculated for the system of MMCs or MMNCs

MMC or MMNC	A356T6–SiC Micro	$Al–Al_2O_3$ Micro	$Mg–Al_2O_3$ Nano
The values of the correction factor (k)	60	14	10^10

Although the model presented here gives slightly better prediction than that of the conventional model [19], both of them show the same trend as the experimental results (Fig. 5). The reason for this point is that these models consider both direct strengthening (load transfer from the matrix to the reinforcement particles) and indirect strengthening (dislocation strengthening) whereas the other models reported in the literature, e.g., strain gradient theory [30], only considered the indirect strengthening.

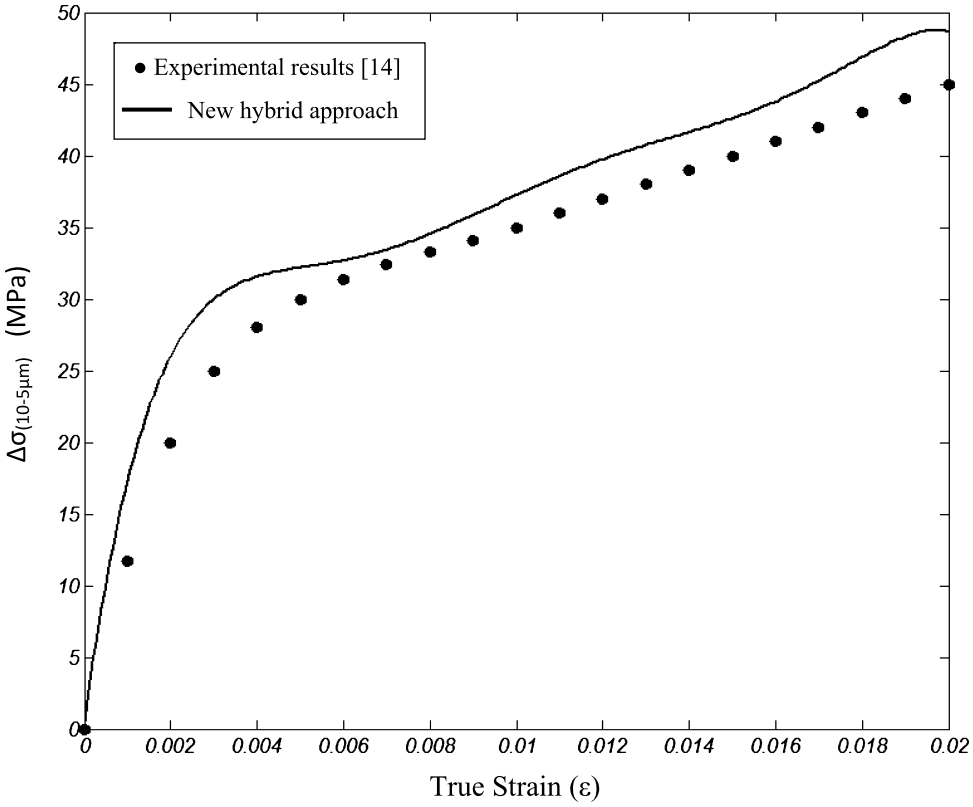

Figure 6. The total incremental increase in yield strength ($\Delta\sigma$) due to decrease of particle size (10–5 μm) *versus* true strain in Al–Al_2O_3 micro-composite and comparison with the experimental results [14].

3.2. *Al/Al_2O_3 Microcomposite*

As another verification of the new model, Al–Al_2O_3 composite has been considered. Figure 6 illustrates both the new model predictions and experimental data [14]. Similarly to the results reported in the previous section, the incremental increase in true yield stress due to decrease of particle size (Al_2O_3) from 10 μm to 5 μm ($\Delta\sigma_{10\text{–}5\ \mu m}$) has been considered as comparison base. In this case, values of the volume fraction (f) and aspect ratio ($2c$) of the reinforcement in the calculations have been considered as 0.4 and 1, respectively. It should be noted that authors in Ref. [14] choose the 0.02% offset stress to characterize the yield point of the composites. Although this is somewhat an arbitrary definition, it allows for comparisons to be made between the various composites. As observed, the new hybrid model shows good accordance with the experimental results but demonstrates a few overestimations. In this matter, two sources of disparity may occur. Foremost, in our model the interactions between the particles have been neglected. To put this another way: we assume a composite containing dilute concentrations of the

filler, the same as Eshelby's equivalent model [31]. In such a composite system, the spacing of particles is large enough that the perturbation of the matrix strain field resulting from each particle vanishes (according to Saint-Vanant's principle) before it can have an effect on any other particles. In this case, each particle behaves as if it is 'isolated', since it cannot sense the presence of its neighbors. This situation is common in nanocomposites since the filler content is usually low. Afterward, in the current model a complete adhesion between the reinforcement and the matrix has been regarded. Incorporating the role of interface in the model can be examined in future works.

3.3. Mg/Al_2O_3 Nanocomposite

The proposed model has a distinctive attribute which can be applied on the MMNCs, additionally. In order to evaluate and compare our modeling results with the conventional proposed model [21, 22], $Mg–Al_2O_3$ nanocomposite has been preferred. Table 3 presents the mechanical and physical properties of the nanocomposite tested at room temperature [32, 33]. The incremental increase in yield stress ($\Delta\sigma$) *versus* particle volume fraction (f) is compared for the new hybrid model and the conventional model [21, 22], as shown in Fig. 7. Calculation in the current model is made based on equation (17) for different sizes of reinforcement nanoparticles (d_p). As stated above, nano-particle size has a significant effect on the yield strength when the volume fraction is slightly higher than 0.01 (Fig. 7). Another important point is that the improvement in the yield strength of the MMNCs becomes very strong when the nano-particle size is smaller than about 100 nm. This is in agreement with the experimental results [33, 34] and provides a theoretical support to the terminology of nanotechnology, e.g., as defined by the U.S. National Science Foundation [35], where "... The novel and differentiating properties and functions are developed at a critical length scale of matter typically under 100 nm ..." is specified. On the other hand, Fig. 7 reveals an enormous disparity between the predicted results using the present model and the conventional model [21, 22]. The major reason for this disparity is consideration of the geometrically dislocation density due to EM mismatch (ρ^{EM}) in our model. In other words, the conventional model only considers the influence of coefficient of thermal expansion (CTE) mismatches between the matrix and the reinforcement on dislocation density (ρ^{CTE}). Also, Fig. 7 shows an intersection point of the conventional model and the new presented model which is called the critical volume fraction (f_c). In the vol-

Table 3.
The mechanical and thermal properties of $Mg–Al_2O_3$ composite [32, 33]

Property	b (°A)	α_p (1/°C)	α_m (1/°C)	$T_{processing}$ (°C)	T_{test} (°C)	μ_m (GPa)	σ_m (MPa)
Values	3.2	9×10^{-6}	28.4×10^{-6}	300	20	16.5	125

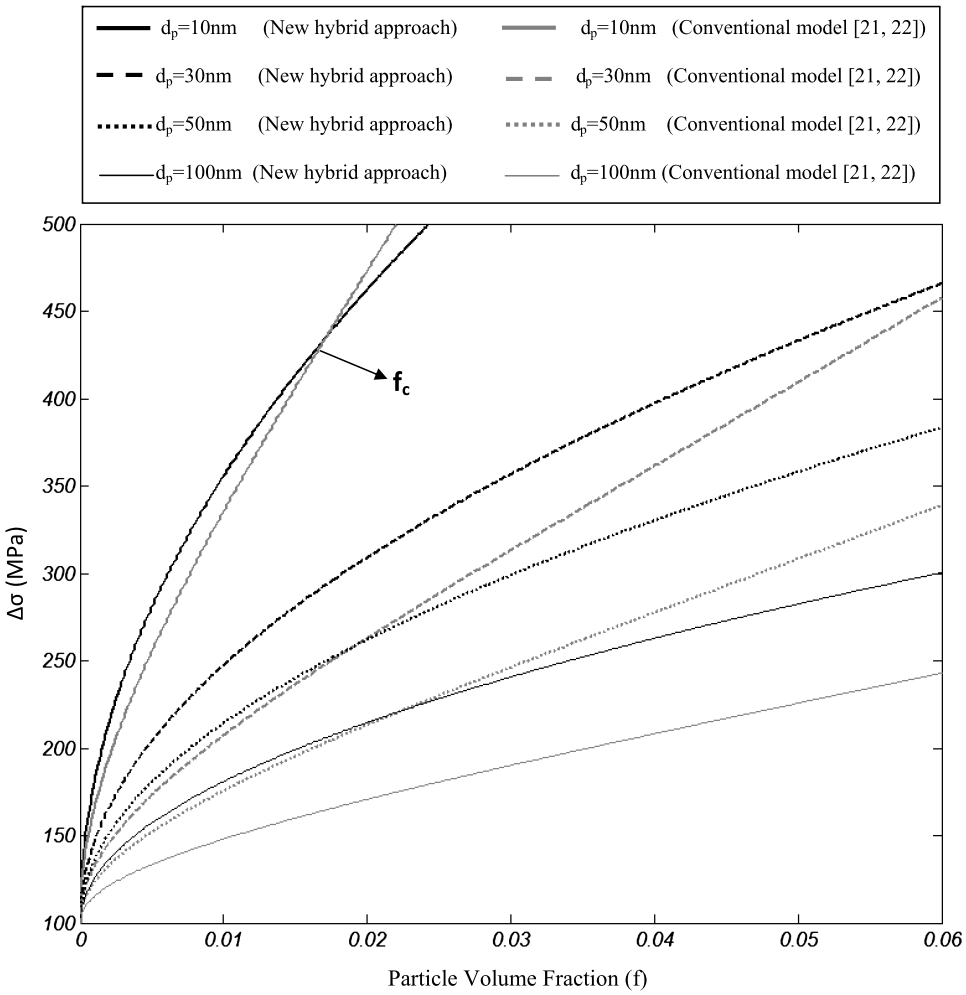

Figure 7. The total incremental increase in yield stress ($\Delta\sigma$) as a function of nano-particle size (d_p) and volume fraction (f) in Mg–Al_2O_3 nanocomposite and comparison with the model proposed by Zhang and Chen [21, 22].

ume fraction smaller than f_c, the presented model in this paper predicts the yield stress much more than the larger f_c and *vice versa* for the conventional model. With decrease in the size of the particles (d_p) and increase in the volume fraction (f), the interception point has been transferred to the smaller volume fraction, which may be due to strong interaction between particles. In fact, the Orowan strengthening mechanism and the geometrical dislocation density mechanism are dominated for $f > f_c$ and $f < f_c$, respectively.

To further verify, another comparison between the present model, the model suggested by Zhang and Chen [21, 22] and the experimental data [32] are presented in Fig. 8. Comparing the present model with the conventional model in this figure il-

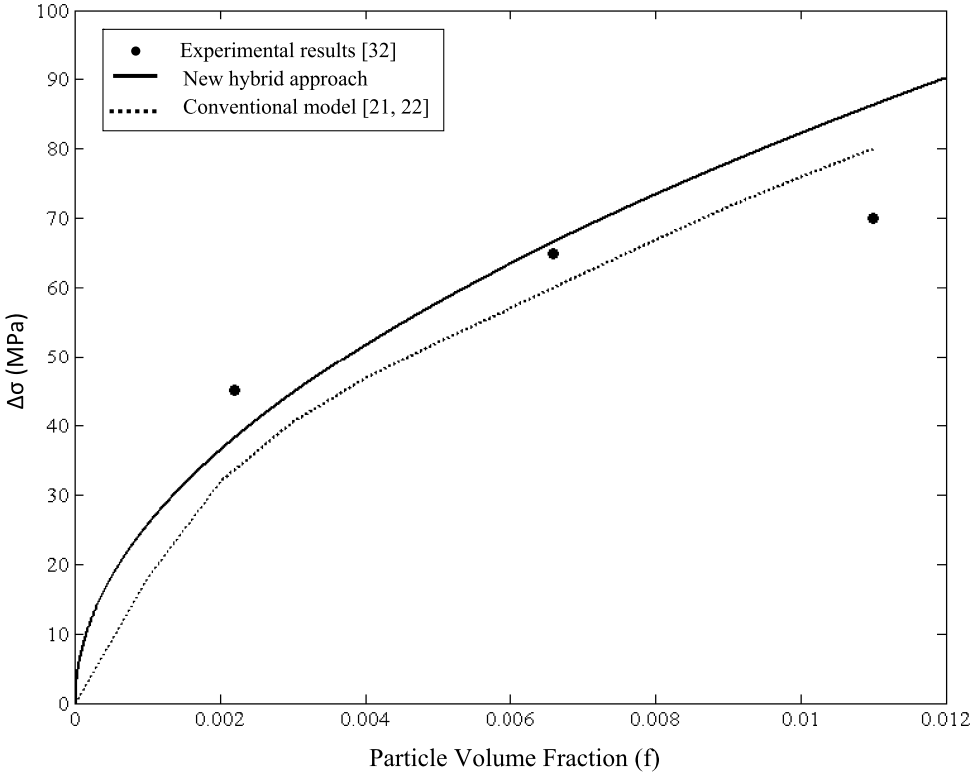

Figure 8. The total incremental increase in yield strength ($\Delta\sigma$) as a function of particle volume fraction (f) in Mg–Al_2O_3 nanocomposite tested at 20°C. Comparisons with the conventional model [21, 22] and experimental results [32] have been made.

lustrates that the present model predicts better results than the conventional model for the smaller volume fractions of fillers (<0.08). However, the present model overestimated the incremental yield stress for the larger volume fractions (>0.08). This overestimation might be due to the fact that in the larger volume fractions, because of some unexpected phenomenon such as agglomeration process, the incremental yield stress decreases. Another superiority of the present model, as stated in Section 2.4, is to consider the aspect ratio ($2c$) as a variable compared to the conventional model [21, 22], particularly in MMNCs systems. This characteristic attribute of the new hybrid approach would have been more obvious if the experimental results were available for the different aspect ratio of the nano-particles. Aspect ratio ($2c$) of the nano-particles has been considered as 1 within our model throughout the above calculations.

4. Conclusions

A multi-scale model to predict the yield strength of MMCs and MMNCs is proposed on the basis of the strengthening effects characterized by the shear lag model

(direct strengthening) and enhanced dislocation density due to elastic modulus (EM) and coefficient of thermal expansion (CTE) mismatches (indirect strengthening). The presented model has two significant attributes which include compatibility (with the best prior models) and flexibility (introducing the aspect ratio of the particles, i.e., $2c$, as a variable). Also, the new hybrid model indicates that 100 nm is a critical size for the particles to improve the yield strength of MMCs; below this the slope of yield strength *versus* particle size increases remarkably. The model shows reasonable agreement with the experimental data reported in the literature, indicating that it is necessary to consider both of the strengthening mechanisms (direct and indirect strengthening).

References

1. S. L. Donaldson and D. B. Miracle, Introduction to composites, in: *ASM Handbook*, Vol. 21. ASM International, Materials Park, OH, USA (2001).
2. C. S. Goh, J. Wei, L. C. Lee and M. Gupta, Properties and deformation behavior of Mg–Y_2O_3 nanocomposites, *Acta Mater*. **55**, 5115–5121 (2007).
3. S. F. Hassan and M. Gupta, Development of nano-Y_2O_3 containing magnesium nanocomposites using solidification processing, *J. Alloys Compos*. **429**, 176–183 (2007).
4. V. D. Castro, T. Leguey, A. Munoz, M. A. Monge and R. Pareja, Relationship between hardness and tensile tests in titanium reinforced with yttria nanoparticles, *Mater. Sci. Engng A* **400**, 345–348 (2005).
5. C. S. Goh, J. Wei, L. C. Lee and M. Gupta, Ductility improvement and fatigue studies in Mg–CNT nanocomposites, *Compos. Sci. Technol*. **68**, 1432–1439 (2008).
6. D. Dean, A. M. Obore, S. Richmon and E. Nyairo, Multiscale fiber-reinforced nanocomposites: synthesis, processing and properties, *Compos. Sci. Technol*. **66**, 2135–2142 (2006).
7. L. Lü, M. O. Lai and W. Liang, Magnesium nanocomposite *via* mechanochemical milling, *Compos. Sci. Technol*. **64**, 2009–2014 (2004).
8. G. E. Dieter, *Mechanical Metallurgy*, 3rd edn. McGraw-Hill Inc., New York, USA (1986).
9. T. Christman, A. Needleman and S. Suresh, An experimental and numerical study of deformation in metal-ceramic composites, *Acta Metall. Mater.* **37**, 3029–3050 (1989).
10. G. Bao, J. W. Hutchinson and R. McMeeking, Particle reinforcement of ductile matrices against plastic flow and creep, *Acta Metall. Mater.* **39**, 1871–1882 (1991).
11. V. C. Nardone and K. M. Prewo, On the strength of discontinuous silicon carbide reinforced aluminum composites, *Scripta Metall*. **20**, 43–48 (1986).
12. L. H. Dai and G. J. Huang, An incremental micromechanical scheme for nonlinear particulate composites, *Intl. J. Mech. Sci*. **43**, 1179–1193 (2001).
13. D. J. Lloyd, Particle reinforced aluminium and magnesium matrix composites, *Intl. Mater. Rev.* **39**, 1–23 (1994).
14. M. Kouzeli and A. Mortensen, Size dependent strengthening in particle reinforced aluminum, *Acta Metall. Mater.* **50**, 39–51 (2002).
15. R. J. Arsenailt and N. Shi, Dislocation generation due to differences between the coefficients of thermal expansion, *Mater. Sci. Engng* **81**, 175–187 (1986).
16. N. Ramakrishnan, An analytical study on strengthening of particulate reinforced metal matrix composites, *Acta Metall. Mater.* **44**, 69–77 (1996).

17. Q. Zhang and D. L. Chen, A model for predicting the particle size dependence of the low cycle fatigue life in discontinuously reinforced MMCs, *Scripta Mater*. **51**, 863–867 (2004).
18. Q. Zhang and D. L. Chen, A model for the low cycle fatigue life prediction of discontinuously reinforced MMCs, *Intl. J. Fatigue* **27**, 417–427 (2005).
19. L. H. Dai, Z. Ling and Y. L. Bai, Size-dependent inelastic behavior of particle-reinforced metal–matrix composites, *Compos. Sci. Technol*. **61**, 1057–1063 (2001).
20. L. F. Liu, L. H. Dai and G. W. Yang, Strain gradient effects on deformation strengthening behavior of particle reinforced metal matrix composites, *Mater. Sci. Engng A* **345**, 190–196 (2003).
21. Z. Zhang and D. L. Chen, Consideration of Orowan strengthening effect in particulate-reinforced metal matrix nanocomposites: a model for predicting their yield strength, *Scripta Mater*. **54**, 1321–1326 (2006).
22. Z. Zhang and D. L. Chen, Contribution of Orowan strengthening effect in particulate-reinforced metal matrix nanocomposites, *Mater. Sci. Engng A* **483**, 148–152 (2008).
23. M. F. Ashby, L. E. Tanner and S. H. Gelles, The stress at which dislocations are generated at a particle–matrix interface, *Phil. Mag*. **19**, 757–771 (1969).
24. M. F. Ashby and L. A. Johnson, On the generation of dislocations at misfitting particles in a ductile matrix, *Phil. Mag*. **20**, 1009–1022 (1969).
25. M. F. Ashby, The deformation of plastically non-homogeneous materials, *Phil. Mag*. **21**, 399–424 (1970).
26. R. J. Arsenault and R. M. Fischer, Microstructure of fiber and particulate SiC in 6061 Al composites, *Scripta Metall*. **17**, 67–71 (1983).
27. T. W. Clyne and P. J. Withers, *An Introduction to Metal Matrix Composites*. Cambridge University Press, Cambridge, UK (1993).
28. R. M. Aikin and L. Christodoulou, The role of equiaxed particles on the yield stress of composites, *Scripta Metall. Mater*. **25**, 9–14 (1991).
29. Z. Ling, Deformation behavior and microstructure effect in 2124Al/SiCp composite, *J. Compos. Mater*. **34**, 101–115 (2000).
30. L. H. Dai, Z. Ling and Y. L. Bai, A strain gradient-strengthening law for particle reinforced metal matrix composites, *Scripta Mater.* **41**, 245–251 (1999).
31. J. D. Eshelby, The determination of the elastic field outside an ellipsoidal inclusion, and related problems, *Proc. Roy. Soc*. **A241**, 376–396 (1957).
32. S. F. Hassan and M. Gupta, Development of high performance magnesium nano-composites using nano-Al_2O_3 as reinforcement, *Mater. Sci. Engng A* **392**, 163–168 (2005).
33. N. Srikanth, S. F. Hassan and M. Gupta, Energy dissipation studies of Mg-based nanocomposites using an innovative circle-fit approach, *J. Compos. Mater*. **38**, 2037–2047 (2004).
34. S. F. Hassan and M. Gupta, Development of high performance magnesium nanocomposites using solidification processing route, *Mater. Sci. Technol*. **20**, 1383–1388 (2004).
35. Available from: www.nsf.gov/home/crssprgm/nano/omb_nifty50.htm.